



**HAL**  
open science

# Understanding the Time-Dependent Effective Diffusion Coefficient Measured by Diffusion MRI: the Intra-Cellular Case

Housseem Haddar, Jing-Rebecca Li, Simona Schiavi

► **To cite this version:**

Housseem Haddar, Jing-Rebecca Li, Simona Schiavi. Understanding the Time-Dependent Effective Diffusion Coefficient Measured by Diffusion MRI: the Intra-Cellular Case. *SIAM Journal on Applied Mathematics*, 2017. hal-01421928

**HAL Id: hal-01421928**

**<https://inria.hal.science/hal-01421928>**

Submitted on 23 Dec 2016

**HAL** is a multi-disciplinary open access archive for the deposit and dissemination of scientific research documents, whether they are published or not. The documents may come from teaching and research institutions in France or abroad, or from public or private research centers.

L'archive ouverte pluridisciplinaire **HAL**, est destinée au dépôt et à la diffusion de documents scientifiques de niveau recherche, publiés ou non, émanant des établissements d'enseignement et de recherche français ou étrangers, des laboratoires publics ou privés.

1                    **UNDERSTANDING THE TIME-DEPENDENT EFFECTIVE**  
2                    **DIFFUSION COEFFICIENT MEASURED BY DIFFUSION MRI: THE**  
3                    **INTRA-CELLULAR CASE\***

4                    HOUSSEM HADDAR<sup>†</sup>, JING-REBECCA LI<sup>†</sup>, AND SIMONA SCHIAVI<sup>†</sup>

5                    **Abstract.** Diffusion Magnetic Resonance Imaging (dMRI) can be used to measure a time-  
6                    dependent effective diffusion coefficient that can in turn reveal information about the tissue geometry.  
7                    Recently a mathematical model for the time-dependent effective diffusion coefficient was obtained  
8                    using homogenization techniques after imposing a certain scaling relationship for the time, the bi-  
9                    ological cell membrane permeability, the diffusion-encoding magnetic field gradient strength, and a  
10                    periodicity length of the cellular geometry. With this choice of the scaling of the physical parameters,  
11                    the effective diffusion coefficient of the medium can be computed after solving a diffusion equation  
12                    subject to a time-dependent Neumann boundary condition, independently in the biological cells and  
13                    in the extra-cellular space. In this paper, we analyze this new model, which we call the H-*ADC*  
14                    model, in the case of finite domains, which is relevant to diffusion inside biological cells. We use both  
15                    the eigenfunction expansion and the single layer potential representation for the solution of the above  
16                    mentioned diffusion equation to obtain analytical expressions for the effective diffusion coefficient in  
17                    different diffusion time regimes. These expressions are validated using numerical simulations in two  
18                    dimensions.

19                    **Key words.** Diffusion MRI; time-dependent *ADC*; homogenization; effective medium;

20                    **AMS subject classifications.** 35B27, 35Q99, 65M32, 65Z05

21                    **1. Introduction.** Diffusion Magnetic Resonance Imaging (dMRI) encodes water  
22                    displacement due to diffusion via the application of diffusion-encoding gradient pulses  
23                    and is a powerful tool to obtain information on the tissue microstructure. A major  
24                    application has been in detecting acute cerebral ischemia minutes after stroke [28, 42].  
25                    DMRI has been used to detect and differentiate a wide range of physiological and  
26                    pathological conditions in the brain, including tumors [25, 37, 40] and myelination  
27                    abnormalities (for a review, see [21]). It also has been used to study brain connectivity  
28                    (for a review, see [20]) and in functional imaging [22] as well as in cardiac applications  
29                    [5, 6, 35].

30                    In particular, we are interested in an important quantity measured by dMRI  
31                    called the “Apparent Diffusion Coefficient” (*ADC*) which is based on a measure of the  
32                    mean diffusion displacement inside an imaging voxel. The mean squared displacment  
33                    of spins during a diffusion time  $t_D$  is defined as:

34                    (1)                     $MSD(t_D) \equiv \frac{1}{\int_{\mathbf{x}_0} \rho(\mathbf{x}_0) d\mathbf{x}_0} \int_{\mathbf{x}_0} \int_{\mathbf{x}} \rho(\mathbf{x}_0) ((\mathbf{x} - \mathbf{x}_0) \cdot \mathbf{u}_{\mathbf{g}})^2 u(\mathbf{x}, \mathbf{x}_0, t_D) d\mathbf{x} d\mathbf{x}_0.$

35                    where  $u(\mathbf{x}, \mathbf{x}_0, t_D)$  is the proportion of spins starting at  $\mathbf{x}_0$  when  $t = 0$  ending up at  
36                    position  $\mathbf{x}$  after a time  $t_D$ ,  $\rho(\mathbf{x}_0)$  is the density of spins at  $\mathbf{x}_0$ , and  $\mathbf{u}_{\mathbf{g}}$  is a unit vector  
37                    in  $\mathbb{R}^3$  ( $\mathbf{u}_{\mathbf{g}}$  is called the diffusion-encoding direction). In the same vein, we can define  
38                    an effective diffusion coefficient in the direction  $\mathbf{u}_{\mathbf{g}}$  by the following expression:

39                    (2)                     $\frac{1}{2 t_D} MSD(t_D).$

---

\*Submitted to the editors December, 10th 2016.

**Funding:** ...

<sup>†</sup>INRIA- CMAP, École Polytechnique, Paris-Saclay ([houssem.haddar@inria.fr](mailto:houssem.haddar@inria.fr), [jingrebecca.li@inria.fr](mailto:jingrebecca.li@inria.fr), [simona.schiavi@polytechnique.edu](mailto:simona.schiavi@polytechnique.edu)).

40 Since the mean squared displacement in a heterogeneous medium is not necessarily  
 41 linear in  $t_D$ , effective diffusion coefficient typically depends on  $t_D$ .

42 The  $MSD$  can be measured by dMRI using a sequence of magnetic field gradient  
 43 pulses (called a diffusion-encoding sequence). A commonly used sequence is the Pulse  
 44 Gradient Spin Echo (PGSE) experiment [36]. In this paper, we will focus on the  
 45 PGSE time profile to simplify the presentation.

46 The PGSE sequence contains two rectangular pulses of the diffusion-encoding  
 47 gradient magnetic field  $B_{\text{diff}} = g\mathbf{u}_g \cdot \mathbf{x}$ , where  $g$  is the strength of the gradient and  
 48  $\mathbf{u}_g$  is the gradient direction. Each pulse has a duration  $\delta$ , with the delay between the  
 49 start of the two pulses denoted  $\Delta$ , and there is also a radio-frequency (RF) pulse to  
 affect a 180 degree spin reversal between the pulses (see Figure 1).

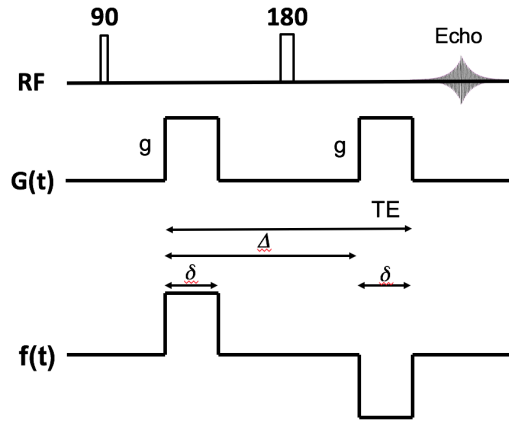


Fig. 1: The Pulsed Gradient Spin Echo (PGSE) sequence. The effective sequence time profile shown here takes into account the 180 degree pulse.

50

51 In the ideal case, where the pulse duration is very short compared to the delay  
 52 between the pulses,  $\delta \ll \Delta$ , called the narrow pulse case, it is easy to relate the  
 53 magnetization of spins to the diffusion propagator  $u(\mathbf{x}, \mathbf{x}_0, t_D)$ . Let us consider spins  
 54 initially located at  $\mathbf{x}_0$ . After the first pulse, the complex phase of these spins is  
 55  $e^{i\delta\gamma\mathbf{g}\cdot\mathbf{x}_0}$ , where  $\gamma = 42.576$  MHz/Tesla is the gyro-magnetic ratio of the water proton.  
 56 Because the gradient magnetic field is turned off after the first pulse, the spins move  
 57 but the phase of the spins does not change. The phase remains  $e^{i\delta\gamma\mathbf{g}\cdot\mathbf{x}_0}$ , until the  
 58 application of the RF pulse resulting in a 180 degree spin reversal. After the 180  
 59 degree RF pulse, the complex phase becomes  $e^{-i\delta\gamma\mathbf{g}\cdot\mathbf{x}_0}$ . Again, spins move but the  
 60 phase of the spins stays the same until the application of the second pulse, after which  
 61 the complex phase due to spins ending up at position  $\mathbf{x}_f$  becomes  $e^{i\delta\gamma\mathbf{g}\cdot(\mathbf{x}_f-\mathbf{x}_0)}$ . So the  
 62 magnetization at position  $\mathbf{x}$  and the echo time  $TE$ , which is the time that the MRI  
 63 signal is acquired, some time after the end of the second pulse ( i.e.  $TE \geq \Delta + \delta$ ), is:

$$64 \quad (3) \quad M(\mathbf{x}, TE) \approx \int_{\mathbf{x}_0} \rho(\mathbf{x}_0) u(\mathbf{x}, \mathbf{x}_0, \Delta) e^{i\delta\gamma\mathbf{g}\cdot(\mathbf{x}-\mathbf{x}_0)} d\mathbf{x}_0,$$

65 where we used the assumption that  $\delta \ll \Delta$ . The dMRI signal  $S$  is the total water

66 proton magnetization in an imaging voxel  $V$ :

$$67 \quad (4) \quad S = \int_{\mathbf{x} \in V} M(\mathbf{x}, TE) d\mathbf{x}.$$

68 Because the diffusion displacement is usually much shorter than the size of the  
69 imaging voxel size we can ignore spins that enter and leave the voxel during the signal  
70 acquisition and thus take domain of integration in Eq. (4) to be  $\mathbb{R}^3$ . Using properties  
71 of the Fourier transform, we obtain

$$72 \quad (5) \quad \left. \frac{\partial \frac{S}{S_0}}{\partial (\delta\gamma g)^2} \right|_{\delta\gamma g=0} \approx MSD(\Delta),$$

73 in the case of the narrow pulse PGSE sequence, where  $S_0$  is the signal at  $g = 0$  (a  
74 derivation of this statement can be found in [23]).

75 Without the narrow pulse assumption, Eq. (3) does not hold exactly. Rather,  
76  $M(\mathbf{x}, t)$  is governed by the Bloch-Torrey equation, which is a complex-valued diffusive  
77 PDE:

$$78 \quad (6) \quad \begin{cases} \frac{\partial}{\partial t} M(\mathbf{x}, t) = -\nu\gamma g \mathbf{u}_{\mathbf{g}} \cdot \mathbf{x} f(t) M(\mathbf{x}, t) + \text{div}(\mathcal{D}_0(\mathbf{x}) \nabla M(\mathbf{x}, t)) & \text{in } \bigcup \Omega_j \times [0, TE] \\ \llbracket \mathcal{D}_0 \nabla M \cdot \nu \rrbracket_{\Gamma_{ij}} = 0 & \text{on } \Gamma_{ij} \times [0, TE] \\ \mathcal{D}_0 \nabla M \cdot \nu|_{\Gamma_{ij}} = \kappa \llbracket M \rrbracket_{\Gamma_{ij}} & \text{on } \Gamma_{ij} \times [0, TE] \\ M(\cdot, 0) = \rho & \text{in } \bigcup \Omega_j \end{cases}$$

79 where  $\Omega_0$  is the extra-cellular space and each of  $\Omega_j$ ,  $j = 1, \dots, N$ , is a biological cell.  
80 The vector  $\nu$  is the exterior normal to the biological cells;  $\llbracket \cdot \rrbracket_{\Gamma_{ij}}$ ,  $i, j = 0, \dots, N$ ,  $i \neq j$ ,  
81 is the jump (the limit value in compartment  $i$  minus the limit value in compartment  $j$ )  
82 on  $\Gamma_{ij}$ , the interface between  $\Omega_i$  and  $\Omega_j$ ;  $\kappa$  is the membrane permeability coefficient;  
83  $\iota$  is the imaginary unit. The function  $f(t)$  gives the normalized time profile of the  
84 diffusion-encoding magnetic field gradient pulses. For the classic Pulsed Gradient  
85 Spin Echo (PGSE) sequence [36], simplified to include only the parameters relevant  
86 to diffusion (the imaging gradients are ignored),

$$87 \quad (7) \quad f(t) = \begin{cases} 1 & t_s < t \leq t_s + \delta, \\ 0 & t_s + \delta < t \leq t_s + \Delta, \\ -1 & t_s + \Delta < t \leq t_s + \Delta + \delta, \\ 0 & \text{elsewhere,} \end{cases}$$

88 where  $t_s$  is the start of the first pulse and we made  $f(t)$  negative in the second pulse  
89 to include the effect of the 180 degree spin reversal between the pulses. For simplicity,  
90 since  $t_s$  does not play a role in the results of this paper, we set  $t_s \rightarrow 0$ . For the same  
91 reason, we set  $TE = \delta + \Delta$  in this paper.

92 We note that the Bloch-Torrey equation needs to be supplemented by additional  
93 boundary conditions on the sides of the imaging voxel. For example, periodic bound-  
94 ary conditions on the boundary of the voxel would be an acceptable choice.

95 In the case of unrestricted diffusion in a homogeneous medium with a diffusion  
96 coefficient  $\mathcal{D}_0$ , the integral of the solution of the Bloch-Torrey equation, in other  
97 words, the total magnetization, takes the following exponential form [4, 16]:

$$98 \quad (8) \quad S = S_0 e^{-\mathcal{D}_0 b},$$

99 with the  $b$ -value defined as:

$$100 \quad (9) \quad b \equiv \gamma^2 g^2 \int_0^{TE} F(t)^2 dt,$$

101 where

$$102 \quad (10) \quad F(t) \equiv \int_0^t f(s) ds.$$

103 In particular, for the PGSE sequence,

$$104 \quad (11) \quad F(t) = \begin{cases} t & t_s < t \leq t_s + \delta, \\ \delta & t_s + \delta < t \leq t_s + \Delta, \\ \Delta + \delta - t & t_s + \Delta < t \leq t_s + \Delta + \delta, \\ 0 & \text{elsewhere.} \end{cases}$$

105 To adapt the definition of the effective diffusion coefficient to the non-narrow  
106 pulse case, we make the following mathematical definition:

$$107 \quad (12) \quad D_{\mathbf{u}_g}^{\text{eff}} \equiv - \frac{1}{\gamma^2 \int_0^{TE} F(t)^2 dt} \frac{\partial}{\partial g^2} \ln \left( \frac{S}{S_0} \right) \Big|_{g=0}.$$

108 In the dMRI community, the above quantity is fitted using the experimental MRI  
109 signal at several  $b$  values and the obtained value is called the ‘‘apparent diffusion  
110 coefficient’’ ( $ADC$ ). The  $ADC$  is widely used medical applications, for instance,  $ADC$   
111 maps of brain have been used to identify tumours (see [21, 41]). The  $D_{\mathbf{u}_g}^{\text{eff}}$  defined  
112 in the above formula depends on the gradient direction  $\mathbf{u}_g$  and the temporal profile  
113  $f(t)$  but not on the gradient amplitude. In this paper, with the phrase ‘‘diffusion  
114 time-dependent’’ we actually mean dependent on  $\Delta$  and  $\delta$ .

115 The motivation of our work is the experimentally observed phenomenon (see [33]  
116 and the references contained there) that the  $ADC$  depends on  $\Delta$  (and  $\delta$  in the non-  
117 narrow pulse case), leading to the need to characterize the time-dependent  $ADC$  in  
118 terms of tissue-related quantities over a wide range of diffusion time regimes. The  
119 ultimate goal is of course the estimation of these tissue-related quantities from the  
120 measured dMRI signal.

121 In this paper, we focus on the case of finite domains, where the membrane per-  
122 meability is small enough to have negligible effect on the effective diffusion coefficient,  
123 which is related to the first order moment of the dMRI signal in the  $b$ -value (Eq. 12).  
124 We note that this does not exclude the permeability from having an effect on the  
125 higher order moments of the signal. For the case where the permeability does affect  
126 the  $D_{\mathbf{u}_g}^{\text{eff}}$ , the analysis is more difficult and we refer the reader to [7, 15, 19, 38, 39]  
127 for results on periodic media and to [3, 8, 30, 31, 32] on more general heterogeneous  
128 media, not necessarily periodic.

129 Now we summarize some existing results concerning the effective diffusion coeffi-  
130 cient for finite domains where the membrane permeability is negligible. In the short  
131 time regime, the effective diffusion coefficient is reduced from the free diffusion coeffi-  
132 cient  $\mathcal{D}_0$  by the presence of the cell membranes that affects only the molecules in the  
133 adjacent layer. The thickness of this layer is of the order of the diffusion length  $\sqrt{\mathcal{D}_0 t}$   
134 [17], where  $\mathcal{D}_0$  is the bulk diffusion coefficient. Calculations in [26, 27] show

$$135 \quad (13) \quad D_{\text{short}}^{\text{eff}}(t) = \mathcal{D}_0 \left( 1 - \frac{4}{3d\sqrt{\pi}} \frac{S}{V} \sqrt{\mathcal{D}_0 t} \right),$$

136 where  $d$  is the spatial dimension and  $S/V$  is the surface to volume ratio. This result  
 137 was extended to include higher order terms accounting for permeable membranes,  
 138 surface relaxation and mean curvature [18, 30]. It was also shown that, in the case of  
 139 anisotropic media subjected to a linear gradient with direction  $\mathbf{u}_g$ , one should replace  
 140  $\frac{S}{dV}$  above by  $\frac{\int_{\partial\Omega}(\mathbf{u}_g \cdot \nu)^2 d\mathbf{x}}{|\Omega|}$  [1, 9]. In the long time limit, the spins explore the whole  
 141 available space of the finite domain and then their mean square displacement saturates  
 142 while the effective diffusion coefficient decreases as  $\Delta$  increases. For an isolated cell  
 143 of a typical size  $R$  the diffusion becomes Gaussian as was shown in [29, 34]. In the  
 144 case of the PGSE sequence in the narrow pulse limit one gets

145 (14) 
$$D_{long}^{eff}(\Delta) \approx C \frac{R^2}{\Delta},$$

146 where  $C$  is a geometrical constant (for example,  $C = 1/4$  for the reflecting cylinder  
 147 and  $C = 1/12$  for a 1D configuration [4, 9]).

148 Finally, an approach that is closely related to the work of this paper is the “ma-  
 149 trix formalism” approach used to describe restricted diffusion in bounded domains[2,  
 150 9, 10, 11]. There one considers the applied diffusion-encoding magnetic field as a per-  
 151 turbation of the Laplace operator and the magnetization is decomposed on the basis  
 152 of Laplacian eigenfunctions.

153 In contrast to the “matrix formalism” approach, the homogeneous model [14]  
 154 which we call the H-ADC model and which is the focus of this paper, was derived  
 155 using a certain scaling of the membrane permeability with respect to other physical  
 156 parameters and thus is not limited to impermeable domains. Our derivation of the  
 157 H-ADC model justifies neglecting the membrane permeability for the choice of scal-  
 158 ing that we have made. In addition, since we have formulated the time-dependent  
 159 effective diffusion coefficient as the solution of a diffusion equation rather than di-  
 160 rectly in the eigenfunction basis, we have the freedom to analyze the solution of the  
 161 resulting diffusion equation using both the eigenfunction representation as well as the  
 162 layer potential representation according the relevant time regime under consideration.  
 163 Finally, we note that we preferred the term “apparent” to the term “effective” in nam-  
 164 ing the H-ADC model due to the more common usage of the term ADC in the MRI  
 165 community.

166 This paper is organized as follows. In Section 2 we describe the H-ADC model  
 167 derived in [14]. In Section 3 we represent the solution of the relevant diffusion equa-  
 168 tion of the H-ADC model using the eigenfunction basis as well as by single layer  
 169 potentials and discuss the regime where each representation is advantageous. In  
 170 Section 4 we provide formulas for the effective diffusion coefficient that is averaged  
 171 over diffusion-encoding gradient directions that are uniformly distributed in the unit  
 172 sphere. In Section 5 we validate our analytical results with numerical simulations on  
 173 two-dimensional geometries. Section 6 contains our conclusions.

174 **2. Effective diffusion coefficient in finite domains.** In a previous work [14],  
 175 we obtained an homogenized model by starting from the Bloch-Torrey equation using  
 176 the following scaling relationship between the time ( $\Delta$  and  $\delta$ ), the biological cell  
 177 membrane permeability ( $\kappa$ ), the diffusion-encoding magnetic field gradient strength  
 178 ( $g$ ), and a periodicity length of the cellular geometry ( $L$ ):

179 
$$L = O(\epsilon), \kappa = O(\epsilon), g = O(\epsilon^{-2}), \{\Delta, \delta\} = O(\epsilon^2),$$

180 where  $\epsilon$  is a non-dimensional parameter. It was shown that with this choice, there  
 181 is no coupling between the different geometrical compartments in the  $g^2$  term which

182 gives rise to the effective diffusion coefficient. The total effective diffusion coefficient  
 183 is the sum of the effective diffusion coefficient in each geometrical compartment  
 184 weighted by its volume fraction. Thus, in this paper we are justified in considering  
 185 each compartment separately.

186 According to [14], with the definitions of  $F(t)$  given in (11), the effective diffusion  
 187 coefficient in the compartment  $\Omega$  can be obtained in the following way:

$$188 \quad (15) \quad D_{\mathbf{u}_g}^{\text{eff}} = \mathcal{D}_0 - \frac{\mathcal{D}_0}{\int_0^{TE} F(t)^2 dt} \int_0^{TE} F(t) h(t) dt,$$

189 where

$$190 \quad (16) \quad h(t) = \frac{1}{|\Omega|} \int_{\Omega} \mathbf{u}_g \cdot \nabla \omega(\mathbf{x}, t)$$

191 is a quantity related to the directional gradient of a function  $\omega$  that is the solution  
 192 of the homogeneous diffusion equation with Neumann boundary condition and zero  
 193 initial condition:

$$194 \quad (17) \quad \begin{aligned} \frac{\partial}{\partial t} \omega(\mathbf{x}, t) - \nabla \cdot (\mathcal{D}_0 \nabla \omega(\mathbf{x}, t)) &= 0, & \mathbf{x} \in \Omega, \\ \mathcal{D}_0 \nabla \omega(\mathbf{x}, t) \cdot \nu(\mathbf{x}) &= \mathcal{D}_0 F(t) \mathbf{u}_g \cdot \nu(\mathbf{x}), & \mathbf{x} \in \partial\Omega, \\ \omega(\mathbf{x}, t) &= 0, & \mathbf{x} \in \Omega, \end{aligned}$$

195  $\nu$  is the outward normal and  $t \in [0, TE]$ . We can see that if  $h(t)$  is close to  $F(t)$ , then  
 196  $D_{\mathbf{u}_g}^{\text{eff}}$  is close to 0. The above set of equations, (15)-(17), comprise the homogenized  
 197 model that we call the H-ADC model.

198 In our previous work [14], we imposed periodic boundary conditions on the bound-  
 199 ary of the voxel. In this paper, we are interested in analyzing (15)-(17) for spatially  
 200 finite compartments, which is relevant to diffusion inside biological cells. It will not  
 201 be necessary to impose periodic boundary conditions on the sides of the imaging voxel  
 202 if we consider only cells that do not touch the sides.

203 **3. Solution of the model.** Defining the right hand side of the Neumann bound-  
 204 ary condition as

$$205 \quad (18) \quad \beta(\mathbf{y}, t) := \mathcal{D}_0 F(t) \mathbf{u}_g \cdot \nu(\mathbf{y}),$$

206 we will use the following two equivalent expressions for  $h(t)$ :

$$207 \quad (19) \quad h(t) = \frac{1}{|\Omega|} \int_{\Omega} \mathbf{u}_g \cdot \nabla \omega(\mathbf{x}, t) d\mathbf{x} = \frac{1}{|\Omega|} \int_{\Gamma} \omega(\mathbf{y}, t) (\mathbf{u}_g \cdot \nu(\mathbf{y})) ds_{\mathbf{y}},$$

208 where the second expression can be obtained by applying the divergence theorem to  
 209 (16). We observe that the first expression uses values of the gradient of  $\omega$  inside  
 210 the domain while the second uses the values of  $\omega$  on the boundary. Each expression  
 211 will have advantages depending on whether we use the eigenfunctions of the Laplace  
 212 operator or layer potentials to represent  $\omega$ .

213 **3.1. Eigenfunctions representation.** Writing  $\omega$  as the sum

$$214 \quad (20) \quad \omega(\mathbf{x}, t) = \tilde{\omega}(\mathbf{x}, t) + F(t) \mathbf{x} \cdot \mathbf{u}_g, \mathbf{x} \in \Omega, t \in [0, TE]$$

215 where  $\tilde{\omega}(\mathbf{x}, t)$  satisfied the diffusion equation with a forcing term and homogeneous  
 216 boundary condition:

$$217 \quad (21) \quad \frac{\partial}{\partial t} \tilde{\omega}(\mathbf{x}, t) - \nabla \cdot (\mathcal{D}_0 \nabla \tilde{\omega}(\mathbf{x}, t)) = -f(t) \mathbf{x} \cdot \mathbf{u}_g, \quad \mathbf{x} \in \Omega, t \in [0, TE],$$

$$218 \quad (22) \quad \mathcal{D}_0 \nabla \tilde{\omega}(\mathbf{x}, t) \cdot \nu(\mathbf{x}) = 0, \quad \mathbf{x} \in \Gamma, t \in [0, TE],$$

$$219 \quad (23) \quad \tilde{\omega}(\mathbf{x}, t) = 0, \quad \mathbf{x} \in \Omega,$$

221 it is well-known that  $\tilde{\omega}(\mathbf{x}, t)$  can be expanded in the basis of Laplace eigenfunctions.  
 222 Let  $\phi_n(\mathbf{x})$  and  $\lambda_n$  be the  $L^2$  normalized eigenfunctions and eigenvalues associated to  
 223 the Laplace operator with homogeneous Neumann boundary conditions:

$$224 \quad -\nabla \mathcal{D}_0 (\nabla \phi_n(\mathbf{x})) = \lambda_n \phi_n(\mathbf{x}), \quad \mathbf{x} \in \Omega,$$

$$225 \quad \mathcal{D}_0 \nabla \phi_n(\mathbf{x}) \cdot \nu(\mathbf{x}) = 0, \quad \mathbf{x} \in \Gamma.$$

227 We can write  $\tilde{\omega}(\mathbf{x}, t)$  in the basis of the eigenfunctions as

$$228 \quad (24) \quad \tilde{\omega}(\mathbf{x}, t) = -a_0 \phi_0(\mathbf{x}) F(t) + \sum_{n=1}^{\infty} (-a_n) \phi_n(\mathbf{x}) \int_0^t e^{-\mathcal{D}_0 \lambda_n (t-s)} f(s) ds,$$

229 where the coefficients are

$$230 \quad (25) \quad a_0 = \frac{1}{\sqrt{|\Omega|}} \int_{\Omega} \mathbf{x} \cdot \mathbf{u}_g d\mathbf{x}, \quad a_n = \int_{\Omega} \mathbf{x} \cdot \mathbf{u}_g \phi_n(\mathbf{x}) d\mathbf{x},$$

232 which coincide with the first moments of the eigenfunctions in the  $\mathbf{u}_g$  direction.

233 Finally, the solution to the diffusion equation is

$$234 \quad (26) \quad \omega(\mathbf{x}, t) = \left( \mathbf{x} \cdot \mathbf{u}_g - \frac{1}{\sqrt{|\Omega|}} a_0 \right) F(t) + \sum_{n=1}^{\infty} (-a_n) \phi_n(\mathbf{x}) \int_0^t e^{-\mathcal{D}_0 \lambda_n (t-s)} f(s) ds$$

235 and using properties of the eigenfunctions:

$$236 \quad (27) \quad \int_{\Omega} \phi_n(\mathbf{x}) d\mathbf{x} = \begin{cases} \sqrt{|\Omega|}, & n = 0 \\ 0, & n \geq 1, \end{cases}$$

237 and the divergence theorem:

$$238 \quad (28) \quad \int_{\Omega} \lambda_n \phi_n(\mathbf{u}_g \cdot \mathbf{x}) d\mathbf{x} = \int_{\Omega} \nabla \phi_n(\mathbf{x}) \cdot \mathbf{u}_g d\mathbf{x} - \int_{\Gamma} \mathcal{D}_0 \nabla \phi_n(\mathbf{x}) \cdot \nu \mathbf{u}_g \cdot \nu ds_{\mathbf{x}} = \int_{\Omega} \nabla \phi_n(\mathbf{x}) \cdot \mathbf{u}_g d\mathbf{x}$$

239 we obtain

$$240 \quad (29) \quad h(t) = F(t) + \sum_{n=1}^{\infty} -\frac{(a_n)^2 \lambda_n}{|\Omega|} \int_0^t e^{-\mathcal{D}_0 \lambda_n (t-s)} f(s) ds.$$

241 This leads to the final formula:

$$242 \quad (30) \quad D_{\mathbf{u}_g}^{\text{eff}} = \sum_{n=1}^{\infty} \frac{(a_n)^2 \mathcal{D}_0 \lambda_n}{|\Omega| \int_0^{TE} F^2(t) dt} \int_0^{TE} F(t) \left( \int_0^t e^{-\mathcal{D}_0 \lambda_n (t-s)} f(s) ds \right) dt.$$

243 We remark that this formula is the same as the one obtained with the matrix formalism  
 244 in [9]. In particular, if we consider PGSE sequence, we can rewrite (15) using the  
 245 contribution of each of the three intervals as  
 (31)

$$246 \quad D_{\mathbf{u}_g}^{\text{eff}} = \mathcal{D}_0 - \left( \underbrace{\frac{\mathcal{D}_0}{A} \int_0^\delta t h(t) dt}_I + \underbrace{\frac{\mathcal{D}_0}{A} \int_\delta^\Delta \delta h(t) dt}_{II} + \underbrace{\frac{\mathcal{D}_0}{A} \int_\Delta^{\Delta+\delta} (\Delta + \delta - t) h(t) dt}_{III} \right),$$

247 where

$$248 \quad (32) \quad A = \int_0^{TE} F^2(t) dt = \delta^2 \left( \Delta - \frac{\delta}{3} \right),$$

249 and in the first pulse

$$250 \quad (33) \quad I = \frac{\mathcal{D}_0 \delta^3}{3A} + \frac{1}{|\Omega|A} \sum_{n=1}^{\infty} (a_n)^2 \left( -\frac{\delta^2}{2} - \frac{\delta e^{-\mathcal{D}_0 \lambda_n \delta}}{\mathcal{D}_0 \lambda_n} - \frac{e^{-\mathcal{D}_0 \lambda_n \delta} - 1}{(\mathcal{D}_0 \lambda_n)^2} \right),$$

252 between the pulses

$$253 \quad (34) \quad II = \frac{\mathcal{D}_0 \delta^2 (\Delta - \delta)}{A} + \frac{1}{|\Omega|A} \sum_{n=1}^{\infty} \frac{-\delta (a_n)^2}{\mathcal{D}_0 \lambda_n} \left( e^{-\mathcal{D}_0 \lambda_n \Delta} - e^{-\mathcal{D}_0 \lambda_n (\Delta - \delta)} - e^{-\mathcal{D}_0 \lambda_n \delta} + 1 \right),$$

255 and in the second pulse

$$257 \quad (35) \quad III = \frac{\mathcal{D}_0 \delta^3}{3A} + \sum_{n=1}^{\infty} \frac{-(a_n)^2}{\mathcal{D}_0 \lambda_n A |\Omega|} \left( \delta - \frac{\delta^2 \mathcal{D}_0 \lambda_n}{2} - \delta e^{-\mathcal{D}_0 \lambda_n \Delta} + \delta e^{-\mathcal{D}_0 \lambda_n (\Delta - \delta)} \right. \\ \left. + \frac{2e^{-\mathcal{D}_0 \lambda_n \Delta} - 1 + e^{-\mathcal{D}_0 \lambda_n \delta} - e^{-\mathcal{D}_0 \lambda_n (\Delta + \delta)} - e^{-\mathcal{D}_0 \lambda_n (\Delta - \delta)}}{\mathcal{D}_0 \lambda_n} \right).$$

260 In the end, we obtain

$$262 \quad (36) \quad D_{\mathbf{u}_g}^{\text{eff}} = \sum_{n=1}^{\infty} \frac{-(a_n)^2}{\mathcal{D}_0^2 \lambda_n^2 \delta^2 \left( \Delta - \frac{\delta}{3} \right) |\Omega|} \left[ e^{-\mathcal{D}_0 \lambda_n (\Delta + \delta)} + e^{-\mathcal{D}_0 \lambda_n (\Delta - \delta)} \right. \\ \left. - 2 \left( \mathcal{D}_0 \lambda_n \delta + e^{-\mathcal{D}_0 \lambda_n \delta} + e^{-\mathcal{D}_0 \lambda_n \Delta} - 1 \right) \right].$$

265 In the narrow pulse case ( $\delta \ll \Delta$ ), we obtain

$$266 \quad (37) \quad D_{\mathbf{u}_g}^{\text{eff}} \approx \sum_{n=1}^{\infty} \frac{(a_n)^2}{\Delta} (1 - e^{-\mathcal{D}_0 \lambda_n \Delta}),$$

267 which confirms that  $D_{\mathbf{u}_g}^{\text{eff}}$  approach its long time limit as proportional to  $1/\Delta$  inside  
 268 finite domains. In particular, for a 1D configuration of length  $L$ ,  $a_1 = \frac{L^2}{12}$  and for a  
 269 reflecting cylinder of radius  $R$ ,  $a_1 = \frac{R^2}{4}$ , which confirm the results in [4, 9].

270 **3.2. Layer potential representation.** The solution of the diffusion equation  
 271 can be also represented using layer potentials [13]. This representation is more efficient  
 272 than the eigenfunction representation at short diffusion times. Since the PDE has a  
 273 Neumann boundary condition, we choose to represent the solution  $\omega(\mathbf{x}, t) = S[\mu](\mathbf{x}, t)$   
 274 as a single layer potential with a density  $\mu$  defined on  $\Gamma$ ,

$$275 \quad (38) \quad S[\mu](\mathbf{x}, t) = \int_0^t \int_{\Gamma} \mathcal{D}_0 G(\mathbf{x} - \mathbf{y}, t - \tau) \mu(\mathbf{y}, \tau) ds_{\mathbf{y}} d\tau,$$

276 where  $G(\mathbf{x}, t)$  is the fundamental solution of the heat equation in free space given by

$$277 \quad (39) \quad G(\mathbf{x}, t) = (4\pi\mathcal{D}_0 t)^{-d/2} \exp\left(\frac{-\|\mathbf{x}\|^2}{4\mathcal{D}_0 t}\right)$$

278 and  $d$  is the space dimension. At short times, there is an unavoidable square root  
 279 singularity in  $t$  in the single layer potential, therefore in what follows, we separate out  
 280 the integrand in (38) in the following way,

$$281 \quad (40) \quad S[\mu](\mathbf{x}, t) = \int_0^t \frac{1}{\sqrt{4\mathcal{D}_0\pi(t-\tau)}} B_S[\mu](\mathbf{x}, t, \tau) d\tau,$$

282 where

$$283 \quad (41) \quad B_S[\mu](\mathbf{x}, t, \tau) := \int_{\Gamma} \mathcal{D}_0 \sqrt{4\mathcal{D}_0\pi(t-\tau)} G(\mathbf{x} - \mathbf{y}, t - \tau) \mu(\mathbf{y}, \tau) ds_{\mathbf{y}}$$

284 is analytic in time if  $\mu$  is. The single layer potential satisfies

$$285 \quad (42) \quad \frac{\partial}{\partial t} S[\mu](\mathbf{x}, t) - \nabla(\mathcal{D}_0 \nabla S[\mu](\mathbf{x}, t)) = 0, \quad \mathbf{x} \in \Omega, t \in [0, TE],$$

$$286 \quad (43) \quad S[\mu](\mathbf{x}, 0) = 0, \quad \mathbf{x} \in \Omega.$$

288 Then the density  $\mu$  is chosen to be a causal function and is determined by imposing  
 289 the Neumann boundary conditions:

$$290 \quad \lim_{\mathbf{x} \rightarrow \mathbf{x}^0 \in \Gamma} \mathcal{D}_0 \nabla S[\mu](\mathbf{x}, t) \cdot \nu(\mathbf{x}) = \beta(\mathbf{x}^0, t), \quad \mathbf{x}^0 \in \Gamma, t \in [0, TE],$$

291 where  $\beta(\mathbf{x}^0, t)$  is defined in (18). Using the jump properties of the traces of double  
 292 layer potentials, the integral equation to be solved for  $\mu$  is then the following:

$$293 \quad (44) \quad \frac{\mathcal{D}_0}{2} \mu(\mathbf{x}^0, t) + \mathcal{D}_0 K^*[\mu](\mathbf{x}^0, t) = \beta(\mathbf{x}^0, t), \quad \mathbf{x}^0 \in \Gamma, t \in [0, TE],$$

294 where

$$295 \quad (45) \quad K^*[\mu](\mathbf{x}^0, t) = \int_0^t \frac{1}{\sqrt{4\pi\mathcal{D}_0(t-\tau)}} B_K[\mu](\mathbf{x}^0, t, \tau) d\tau,$$

297 with

$$298 \quad (46) \quad B_K[\mu](\mathbf{x}^0, t, \tau) \equiv \int_{\Gamma} \frac{-2(\mathbf{x}^0 - \mathbf{y}) \cdot \nu(\mathbf{y})}{4\mathcal{D}_0(t-\tau)} \mathcal{D}_0 \sqrt{4\pi\mathcal{D}_0(t-\tau)} G(\mathbf{x}^0 - \mathbf{y}, t - \tau) \mu(\mathbf{y}, \tau) ds_{\mathbf{y}}$$



331 and for the operator  $K^*$  it was shown that:

(53)

$$\begin{aligned}
 B_K[\mu](\mathbf{x}^0, t, \tau) &= \frac{\gamma_{ss}(\mathbf{x}^0)}{2} \mu(\mathbf{x}^0, t) + \frac{1}{8} \left[ 16\gamma_{sss}(\mathbf{x}^0) \mu_s(\mathbf{x}^0, t) + 12\gamma_{ss}(\mathbf{x}^0) \mu_{ss}(\mathbf{x}^0, t) \right. \\
 &+ 4\gamma_{ss}(\mathbf{x}^0) \mu_t(\mathbf{x}^0, t) + (6\gamma_{ssss}(\mathbf{x}^0) - 15\gamma_{ss}(\mathbf{x}^0)^3) \mu(\mathbf{x}^0, t) \left. \right] (t - \tau) \\
 &+ O((t - \tau)^2).
 \end{aligned}$$

333 Specifically  $\gamma_{ss}$  is the curvature of  $\Gamma$  at the point  $\mathbf{x}^0$  and in what follows we will  
 334 indicate it as  $k(\mathbf{x}^0)$ . In three dimensions, it should be easy to see that the constant  
 335 term in  $B_S[\mu](\mathbf{x}^0, t, \tau)$  would not change, and the constant term in  $B_K[\mu](\mathbf{x}^0, t, \tau)$   
 336 would contain spatial derivatives on a two dimensional manifold.

337 For the PGSE sequence,  $\beta(\mathbf{x}^0, t)$  assumes the following three expressions in the  
 338 three time intervals:

$$(54) \quad \beta(\mathbf{x}^0, t) = \mathcal{D}_0 \mathbf{u}_g \cdot \nu(\mathbf{x}^0) \begin{cases} t & 0 < t \leq \delta, \\ \delta & \delta < t \leq \Delta, \\ \Delta + \delta - t & \Delta < t \leq \Delta + \delta. \end{cases}$$

340 First, using the definition (40) and the result (52) we obtain

$$\begin{aligned}
 S \left[ \frac{2}{\mathcal{D}_0} \beta \right] (\mathbf{x}^0, t) &= \frac{4(\mathcal{D}_0)^{1/2}}{3\sqrt{\pi}} \mathbf{u}_g \cdot \nu(\mathbf{x}^0) \begin{cases} t^{3/2} \\ t^{3/2} - (t - \delta)^{3/2} \\ t^{3/2} - (t - \delta)^{3/2} - (t - \Delta)^{3/2} \end{cases} \\
 (55) \quad &+ O \left\{ \begin{cases} (t^{5/2}) & \text{if } 0 < t \leq \delta, \\ (t^{5/2} - (t - \delta)^{5/2}) & \text{if } \delta < t \leq \Delta, \\ (t^{5/2} - (t - \delta)^{5/2} - (t - \Delta)^{5/2}) & \text{if } \Delta < t \leq \Delta + \delta. \end{cases} \right.
 \end{aligned}$$

342 Similarly, using the definition (45) and the result (53) we obtain

$$(56) \quad K^*[\beta](\mathbf{x}^0, t) = \alpha_1(\mathbf{x}_0) \alpha_2(t) + O(\alpha_3(t))$$

344 where

$$\begin{aligned}
 \alpha_1(\mathbf{x}_0) &= \frac{(\mathcal{D}_0)^{3/2} k(\mathbf{x}^0)}{3\sqrt{\pi}} (\mathbf{u}_g \cdot \nu(\mathbf{x}^0)), \\
 \alpha_2(t) &= \begin{cases} t^{3/2} & \text{if } 0 < t \leq \delta, \\ t^{3/2} - (t - \delta)^{3/2} & \text{if } \delta < t \leq \Delta, \\ t^{3/2} - (t - \delta)^{3/2} - (t - \Delta)^{3/2} & \text{if } \Delta < t \leq \Delta + \delta, \end{cases} \\
 (57) \quad \alpha_3(t) &= \begin{cases} t^{5/2} & \text{if } 0 < t \leq \delta, \\ t^{5/2} - (t - \delta)^{5/2} & \text{if } \delta < t \leq \Delta, \\ t^{5/2} - (t - \delta)^{5/2} - (t - \Delta)^{5/2} & \text{if } \Delta < t \leq \Delta + \delta. \end{cases}
 \end{aligned}$$

346 To compute  $S \left[ -\frac{4}{\mathcal{D}_0} K^*[\beta] \right] (\mathbf{x}^0, t)$ , we first observe that  $S \left[ -\frac{4}{\mathcal{D}_0} K^*[\beta] \right] (\mathbf{x}^0, t) = -\frac{4}{\mathcal{D}_0} S [K^*[\beta]] (\mathbf{x}^0, t)$ .

347 Moreover, to compute  $S [K^*[\beta]] (\mathbf{x}^0, t)$  we cannot use the result (52) because  $\alpha_2$  and

348  $\alpha_3$  do not have a Taylor expansion in  $t$ . Following the idea in [12], we explicitly  
 349 compute the lowest order terms of  $S[K^*[\beta]](\mathbf{x}^0, t)$  in two dimensions by

$$350 \quad (58) \quad S[K^*[\beta]](\mathbf{x}_0, t) = \int_0^t \frac{1}{\sqrt{4\pi\mathcal{D}_0(t-\tau)}} B_S[K^*[\beta]](\mathbf{x}_0, t, \tau) d\tau,$$

351 where

$$352 \quad (59) \quad \begin{aligned} & B_S[K^*[\beta]](\mathbf{x}_0, t, \tau) \\ &= \int_{-\infty}^{+\infty} \mathcal{D}_0 \frac{e^{-\frac{s^2+y(s)^2}{4\mathcal{D}_0(t-\tau)}}}{\sqrt{4\pi\mathcal{D}_0(t-\tau)}} (\alpha_1(s)\alpha_2(\tau) + O(\alpha_3(\tau))) \sqrt{1+(y'(s))^2} ds. \end{aligned}$$

353 Note for simplicity, we replaced  $\alpha_1(\mathbf{x}_0)$  by  $\alpha_1(s)$  to indicate the local parametrization  
 354 of  $\Gamma$  around  $\mathbf{x}_0$ , as described previously.

355 To compute the above spatial integral we note the dominant contribution of the  
 356 Gaussian  $e^{-\frac{s^2}{4\mathcal{D}_0(t-\tau)}}$  and make the change of variables  $r = \frac{s}{\sqrt{4\mathcal{D}_0(t-\tau)}}$  to obtain

$$357 \quad \begin{aligned} B_S[K^*[\beta]](\mathbf{x}_0, t, \tau) &= \int_{-\infty}^{+\infty} \frac{\mathcal{D}_0}{\sqrt{\pi}} e^{-r^2} e^{-\frac{y(rv)^2}{v^2}} \\ &\left( \alpha_1(rv)\alpha_2\left(t - \frac{v^2}{4\mathcal{D}_0}\right) + O\left(\alpha_3\left(t - \frac{v^2}{4\mathcal{D}_0}\right)\right) \right) \sqrt{1+(y'(rv))^2} dr, \end{aligned}$$

358 where  $v = \sqrt{4\mathcal{D}_0(t-\tau)}$ . We would like an asymptotic expansion of the above integral  
 359 in  $v$ . We note  $y(rv) = \frac{1}{2}k(\mathbf{x}_0)r^2v^2 + O(r^3v^3)$  and  $\alpha_1(0) = \frac{(\mathcal{D}_0)^{3/2}k(\mathbf{x}^0)}{3\sqrt{\pi}} (\mathbf{u}_{\mathbf{g}} \cdot \nu(\mathbf{x}^0))$ .  
 360 The order  $O(v)$  term only occurs in  $\alpha_1$  and we do not need to take it into account  
 361 due to the anti-symmetry of  $e^{-r^2}r$ . So we compute the space integral to obtain

$$362 \quad \begin{aligned} &= \int_{-\infty}^{+\infty} \frac{\mathcal{D}_0}{\sqrt{\pi}} e^{-r^2} \left( (\alpha_1(0) + O(r^2v^2)) \alpha_2\left(t - \frac{v^2}{4\mathcal{D}_0}\right) + O\left(\alpha_3\left(t - \frac{v^2}{4\mathcal{D}_0}\right)\right) \right) dr \\ &= \alpha_2\left(t - \frac{v^2}{4\mathcal{D}_0}\right) (\mathcal{D}_0\alpha_1(0) + O(v^2)) + O\left(\alpha_3\left(t - \frac{v^2}{4\mathcal{D}_0}\right)\right). \end{aligned}$$

363 We now take the above expression and put it into the time integral to get  
 364  $S[K^*[\beta]](\mathbf{x}_0, t)$ :

$$365 \quad \int_0^t \frac{1}{\sqrt{4\pi\mathcal{D}_0(t-\tau)}} (\alpha_2(\tau) (\mathcal{D}_0\alpha_1(0) + O(t-\tau)) + O(\alpha_3(\tau))) d\tau.$$

366 Using the following property of the beta function (the Euler integral of the first kind)

$$367 \quad \int_0^t (t-\tau)^w \tau^p d\tau = t^{p+w+1} \frac{\Gamma(p+1)\Gamma(w+1)}{\Gamma(w+p+2)},$$

368 we can compute  $\int_0^t \frac{1}{\sqrt{(t-\tau)}} \alpha_2(\tau) d\tau$  exactly:

$$\begin{aligned}
 & \int_0^t \frac{\tau^{\frac{3}{2}}}{\sqrt{t-\tau}} d\tau = \frac{3\pi}{8} t^2, \\
 369 \quad (60) \quad & \int_0^\delta \frac{\tau^{\frac{3}{2}}}{\sqrt{t-\tau}} d\tau + \int_\delta^t \frac{\tau^{\frac{3}{2}} - (\tau-\delta)^{\frac{3}{2}}}{\sqrt{t-\tau}} d\tau = \frac{3\pi}{8} (t^2 - (t-\delta)^2) \\
 & \int_0^\delta \frac{\tau^{\frac{3}{2}}}{\sqrt{t-\tau}} d\tau + \int_\delta^\Delta \frac{\tau^{\frac{3}{2}} - (\tau-\delta)^{\frac{3}{2}}}{\sqrt{t-\tau}} d\tau + \int_\Delta^t \frac{\tau^{\frac{3}{2}} - (\tau-\delta)^{\frac{3}{2}} - (\tau-\Delta)^{\frac{3}{2}}}{\sqrt{t-\tau}} d\tau \\
 & = \frac{3\pi}{8} (t^2 - (t-\delta)^2 - (t-\Delta)^2).
 \end{aligned}$$

370 Therefore, the dominant asymptotic terms are:

$$\begin{aligned}
 (61) \quad & S \left[ -\frac{4}{\mathcal{D}_0} K^*[\beta] \right] (\mathbf{x}^0, t) = -\frac{4}{\mathcal{D}_0} \frac{\mathcal{D}_0^2}{16} k(\mathbf{x}^0) (\mathbf{u}_{\mathbf{g}} \cdot \nu(\mathbf{x}^0)) \begin{cases} t^2 \\ t^2 - (t-\delta)^2 \\ t^2 - (t-\delta)^2 - (t-\Delta)^2. \end{cases} \\
 371 \quad & + O \begin{cases} (t^3) & \text{if } 0 < t \leq \delta, \\ (t^3 - (t-\delta)^3), & \text{if } \delta < t \leq \Delta, \\ (t^3 - (t-\delta)^3 - (t-\Delta)^3) & \text{if } \Delta < t \leq \Delta + \delta, \end{cases}
 \end{aligned}$$

372 where we computed the error term by evaluating  $\int_0^t \frac{1}{\sqrt{(t-\tau)}} \alpha_2(\tau) (t-\tau) d\tau$  and

373  $\int_0^t \frac{1}{\sqrt{(t-\tau)}} \alpha_3(\tau) d\tau$ , again using property of the beta function. Namely, for

374  $\int_0^t \frac{1}{\sqrt{(t-\tau)}} \alpha_2(\tau) (t-\tau) d\tau$ , we have

$$\begin{aligned}
 & \int_0^t \frac{\tau^{\frac{3}{2}}}{\sqrt{t-\tau}} (t-\tau) d\tau = \frac{\pi}{16} t^3, \\
 & \int_0^\delta \frac{\tau^{\frac{3}{2}}}{\sqrt{t-\tau}} (t-\tau) d\tau + \int_\delta^t \frac{\tau^{\frac{3}{2}} - (\tau-\delta)^{\frac{3}{2}}}{\sqrt{t-\tau}} (t-\tau) d\tau = \frac{\pi}{16} (t^3 - (t-\delta)^3) \\
 375 \quad (62) \quad & \int_0^\delta \frac{\tau^{\frac{3}{2}}}{\sqrt{t-\tau}} (t-\tau) d\tau + \int_\delta^\Delta \frac{\tau^{\frac{3}{2}} - (\tau-\delta)^{\frac{3}{2}}}{\sqrt{t-\tau}} (t-\tau) d\tau \\
 & + \int_\Delta^t \frac{\tau^{\frac{3}{2}} - (\tau-\delta)^{\frac{3}{2}} - (\tau-\Delta)^{\frac{3}{2}}}{\sqrt{t-\tau}} (t-\tau) d\tau \\
 & = \frac{\pi}{16} (t^3 - (t-\delta)^3 - (t-\Delta)^3).
 \end{aligned}$$

376 For  $\int_0^t \frac{1}{\sqrt{t-\tau}} \alpha_3(\tau) d\tau$ , we have

$$\begin{aligned}
& \int_0^t \frac{\tau^{\frac{5}{2}}}{\sqrt{t-\tau}} d\tau = \frac{5\pi}{16} t^3, \\
& \int_0^\delta \frac{\tau^{\frac{5}{2}}}{\sqrt{t-\tau}} d\tau + \int_\delta^t \frac{\tau^{\frac{5}{2}} - (\tau-\delta)^{\frac{3}{2}}}{\sqrt{t-\tau}} d\tau = \frac{5\pi}{16} (t^3 - (t-\delta)^3) \\
& \int_0^\delta \frac{\tau^{\frac{5}{2}}}{\sqrt{t-\tau}} d\tau + \int_\delta^\Delta \frac{\tau^{\frac{5}{2}} - (\tau-\delta)^{\frac{5}{2}}}{\sqrt{t-\tau}} d\tau + \int_\Delta^t \frac{\tau^{\frac{5}{2}} - (\tau-\delta)^{\frac{5}{2}} - (\tau-\Delta)^{\frac{5}{2}}}{\sqrt{t-\tau}} d\tau \\
& = \frac{5\pi}{16} (t^3 - (t-\delta)^3 - (t-\Delta)^3).
\end{aligned}
\tag{63}$$

378 Replacing the various expressions in (50) with the calculations we did above, we  
379 obtain the approximation with the error bound:

$$\begin{aligned}
S[\mu](\mathbf{x}^0, t) &= \frac{4(\mathcal{D}_0)^{1/2}}{3\sqrt{\pi}} \mathbf{u}_g \cdot \nu(\mathbf{x}^0) \begin{cases} t^{3/2} \\ t^{3/2} - (t-\delta)^{3/2} \\ t^{3/2} - (t-\delta)^{3/2} - (t-\Delta)^{3/2} \end{cases} \\
& - \frac{\mathcal{D}_0}{16} k(\mathbf{x}^0) (\mathbf{u}_g \cdot \nu(\mathbf{x}^0)) \begin{cases} t^2 \\ t^2 - (t-\delta)^2 \\ t^2 - (t-\delta)^2 - (t-\Delta)^2 \end{cases} + \text{higher order terms.}
\end{aligned}
\tag{64}$$

381 Now using (64) we compute the approximate expressions of  $h(t)$  in each time-interval  
382 with the corresponding errors in time.

383 In the first interval, we obtain

$$384 \quad (65) \quad h(t) = \frac{1}{|\Omega|} \int_\Gamma \omega(\mathbf{x}, t) (\mathbf{u}_g \cdot \nu(\mathbf{x})) ds_{\mathbf{x}} = P t^{3/2} + O(P_{\text{err}} t^2),$$

385 where

$$386 \quad (66) \quad P = \frac{1}{|\Omega|} \int_\Gamma \left( \frac{4}{3\sqrt{\pi}} \sqrt{\mathcal{D}_0} (\mathbf{u}_g \cdot \nu(\mathbf{x})) \right)^2 ds_{\mathbf{x}}$$

$$387 \quad (67) \quad P_{\text{err}} = -\frac{\mathcal{D}_0}{4|\Omega|} \int_\Gamma k(\mathbf{x}) (\mathbf{u}_g \cdot \nu(\mathbf{x}))^2 ds_{\mathbf{x}}$$

388 and  
389

$$390 \quad (68) \quad I = \frac{\mathcal{D}_0}{\delta^2 (\Delta - \frac{\delta}{3})} \int_0^\delta t h(t) dt = \frac{2\mathcal{D}_0 P}{7 (\Delta - \frac{\delta}{3})} \delta^{7/2} + O\left(\mathcal{D}_0 P_{\text{err}} \frac{\delta^2}{4 (\Delta - \frac{\delta}{3})}\right).$$

391 Between the pulses, we obtain

$$392 \quad (69) \quad h(t) = \frac{1}{|\Omega|} \int_\Gamma \omega(\mathbf{x}, t) (\mathbf{u}_g \cdot \nu(\mathbf{x})) ds_{\mathbf{x}} = P (t^{3/2} - (t-\delta)^{3/2}) + O(P_{\text{err}} (t^2 - (t-\delta)^2))$$

393 and

$$\begin{aligned}
394 \quad (70) \quad II &= \frac{\mathcal{D}_0}{\delta^2 (\Delta - \frac{\delta}{3})} \int_\delta^\Delta \delta h(t) dt = -\frac{2}{5} \frac{\mathcal{D}_0 P (\delta^{7/2} - \Delta^{5/2} \delta + (\Delta - \delta)^{5/2} \delta)}{\delta^2 (\Delta - \frac{\delta}{3})} \\
& + O\left(\mathcal{D}_0 P_{\text{err}} \left(\frac{\Delta^2 - \delta \Delta}{\Delta - \frac{\delta}{3}}\right)\right).
\end{aligned}$$

396

397 During the second pulse, we find

$$398 \quad h(t) = \frac{1}{|\Omega|} \int_{\Gamma} \omega(\mathbf{x}, t) (\mathbf{u}_{\mathbf{g}} \cdot \nu(\mathbf{x})) ds_{\mathbf{x}} = P \left( t^{3/2} - (t - \delta)^{3/2} - (t - \Delta)^{3/2} \right) \\ 399 \quad + O \left( P_{\text{err}} (t^2 - (t - \delta)^2 - (t - \Delta)^2) \right) \\ 400 \quad (71)$$

401 and

$$402 \quad III = \frac{\mathcal{D}_0}{\delta^2 \left( \Delta - \frac{\delta}{3} \right)} \int_{\Delta}^{\Delta + \delta} (\Delta + \delta - t) h(t) dt \\ 403 \quad = \frac{2}{35} \frac{\mathcal{D}_0 P}{\delta^2 \left( \Delta - \frac{\delta}{3} \right)} \left( (2\Delta^3 + \Delta^2 \delta - 8\Delta \delta^2 + 5\delta^3) \sqrt{\Delta - \delta} + 2(\Delta + \delta)^{7/2} \right. \\ 404 \quad \left. - 4\Delta^{7/2} - 7\Delta^{5/2} \delta - 2\delta^{7/2} \right) + O \left( \mathcal{D}_0 P_{\text{err}} \left( \frac{\Delta \delta - \frac{1}{4} \delta^2}{\Delta - \frac{\delta}{3}} \right) \right). \\ 405 \quad (72)$$

406 Finally, adding up the above expressions, we obtain that using the layer potentials  
407 representation,

$$408 \quad D_{\mathbf{u}_{\mathbf{g}}}^{\text{eff}} = \mathcal{D}_0 \left[ 1 - \frac{4}{35} \frac{P}{\delta^2 \left( \Delta - \frac{\delta}{3} \right)} \left( (\Delta + \delta)^{7/2} - 2 \left( \delta^{7/2} + \Delta^{7/2} \right) + (\Delta - \delta)^{7/2} \right) \right] \\ 409 \quad + O \left( \mathcal{D}_0 P_{\text{err}} \frac{\Delta^2}{\Delta - \frac{\delta}{3}} \right), \\ 410 \quad (74)$$

411 with  $P$  and  $P_{\text{err}}$  defined in (66) and (67), respectively.

412 We observe that, in the narrow pulse limit,  $\delta \ll \Delta$ , the expression (73)

$$413 \quad D_{\mathbf{u}_{\mathbf{g}}}^{\text{eff}} = \mathcal{D}_0 \left( 1 - \frac{4}{3\sqrt{\pi}} \sqrt{\mathcal{D}_0 \Delta} \frac{\int_{\Gamma} (\mathbf{u}_{\mathbf{g}} \cdot \nu)^2 ds_{\mathbf{x}}}{|\Omega|} \right) + O(\mathcal{D}_0 P_{\text{err}} \Delta), \\ 414$$

415 reduces to the formula given in [1, 9]. If  $\Omega$  is an isotropic domain, then

$$416 \quad (75) \quad \frac{\int_{\Gamma} (\mathbf{u}_{\mathbf{g}} \cdot \nu)^2 ds_{\mathbf{x}}}{|\Omega|} = \frac{|\Gamma|}{d|\Omega|},$$

417 which is the ratio of surface to volume divided by the space dimension  $d$ , exactly  
418 the quantity contained in the formula in [27]. Hence our new formula in (73) is a  
419 correction of the results in [1, 9, 27] because it takes into account the contribution of  
420  $\delta$ . This makes the new formula applicable for cases where the narrow pulse assumption  
421  $\delta \ll \Delta$  does not hold. Of course, this description still hold only for short times due  
422 to the nature of the asymptotic expansions for layer potentials.

423 **3.3. Mixed approximation.** When the pulses are short but the delay between  
424 the pulses is not short (with respect to diffusion in  $\Omega$ ), we use the single layer potential  
425 representation in the first and third intervals and the eigenfunction representation  
426 between the pulses.

427 In the first pulse,  $t \in [0, \delta]$ , we have the same results as in the previous section,  
428 namely,

$$429 \quad (76) \quad I = \frac{8}{21A|\Omega|\sqrt{\pi}} \mathcal{D}_0^{3/2} \delta^{7/2} \int_{\Gamma} (\mathbf{u}_{\mathbf{g}} \cdot \nu)^2 ds_{\mathbf{x}} + O \left( \frac{\delta^2}{\left( \Delta - \frac{\delta}{3} \right)} \right).$$





490 where  $\omega_{\mathbf{u}_g}(\mathbf{x}, t)$  solves the problem (17). Because of the linearity of the Neumann  
491 problem, for every direction  $\mathbf{u}_g = [u_1, \dots, u_d]$  we have that

$$492 \quad (94) \quad \omega_{\mathbf{u}_g}(\mathbf{x}, t) = \sum_{i=1}^d u_i \omega_{\mathbf{e}_i}(\mathbf{x}, t),$$

493 where  $\mathbf{e}_i$  is the  $i$ -th vector of the canonical basis of  $\mathbb{R}^d$ . As a consequence

$$494 \quad D_{\mathbf{u}_g}^{\text{eff}} = \mathcal{D}_0 - \frac{\mathcal{D}_0}{A|\Omega|} \int_0^{TE} F \int_{\Omega} (u_1 \mathbf{e}_1 + \dots + u_d \mathbf{e}_d) \cdot (u_1 \nabla \omega_{\mathbf{e}_1} + \dots + u_d \nabla \omega_{\mathbf{e}_d}) d\mathbf{x} dt$$

$$495 \quad = \mathcal{D}_0 - \frac{\mathcal{D}_0}{A|\Omega|} \int_0^{TE} F \left( \sum_{i=1}^d u_i^2 \int_{\Omega} \mathbf{e}_i \cdot \nabla \omega_{\mathbf{e}_i} d\mathbf{x} + \sum_{\substack{i \neq j \\ i, j=1}}^d u_i u_j \int_{\Omega} \mathbf{e}_i \cdot \nabla \omega_{\mathbf{e}_j} d\mathbf{x} \right) dt$$

497 and thus, if we want to average over all the possible directions, we are interested in  
498 the integrals

$$499 \quad (95) \quad \frac{\int_{\mathbb{S}^{d-1}} u_i^2 d\mathbf{u}}{\int_{\mathbb{S}^{d-1}} d\mathbf{u}}, \quad i = 1, \dots, d \quad \text{and} \quad \frac{\int_{\mathbb{S}^{d-1}} u_i u_j d\mathbf{u}}{\int_{\mathbb{S}^{d-1}} d\mathbf{u}}, \quad i, j = 1, \dots, d, i \neq j.$$

500 We observe that, for all  $i, j = 1, \dots, d$  and  $i \neq j$ ,

$$501 \quad (96) \quad \int_{\mathbb{S}^{d-1}} u_i u_j d\mathbf{u} = 0.$$

502 Therefore, what remains in the average are just the terms

$$503 \quad (97) \quad \sum_{i=1}^d \frac{\int_{\mathbb{S}^{d-1}} u_i^2 d\mathbf{u}}{\int_{\mathbb{S}^{d-1}} d\mathbf{u}} \int_{\Omega} \mathbf{e}_i \cdot \nabla \omega_{\mathbf{e}_i} d\mathbf{x},$$

504 i.e. simply the average over  $d$  perpendicular directions and then

$$505 \quad (98) \quad D_{\text{ave}}^{\text{eff}} = \mathcal{D}_0 - \sum_{i=1}^d \frac{\mathcal{D}_0}{dA|\Omega|} \int_0^{TE} F(t) \int_{\Omega} \mathbf{u}_g^i \cdot \nabla \omega_{\mathbf{u}_g^i}(\mathbf{x}, t) d\mathbf{x} dt$$

506 where  $\mathbf{u}_g^i, i = 1, \dots, d$  are  $d$  orthogonal directions. In short, averaging over all the  
507 possible directions is equivalent to average only over  $d$  orthogonal normalized direc-  
508 tions.

509 We use the fact that

$$510 \quad (99) \quad \sum_{i=1}^d \frac{\int_{\Gamma} (\mathbf{u}_g^i \cdot \nu)^2 ds_{\mathbf{x}}}{d} = \frac{|\Gamma|}{d}$$

511 and we define

$$512 \quad (100) \quad k_n := \sum_{i=1}^d \frac{-(a_n^i)^2}{d|\Omega|} = \sum_{i=1}^d \frac{-(\int_{\Omega} \mathbf{x} \cdot \mathbf{u}_g^i \phi_n(\mathbf{x}) d\mathbf{x})^2}{d|\Omega|} d\mathbf{u}_g,$$

513 i.e. the mean over  $d$  orthogonal directions of the square of the first moment along  
514 these directions, and

$$515 \quad (101) \quad j_n := \sum_{i=1}^d \frac{b_n^i a_n^i}{d|\Omega|} = \sum_{i=1}^d \frac{(\int_{\Omega} \omega_{\mathbf{u}_g^i}(\mathbf{x}, \delta) \phi_n(\mathbf{x}) d\mathbf{x}) (\int_{\Omega} \mathbf{x} \cdot \mathbf{u}_g^i \phi_n(\mathbf{x}) d\mathbf{x})}{d|\Omega|}.$$

516 In summary, the eigenfunction expansion in (36) gives  
 517

$$518 \quad (102) \quad D_{ave}^{\text{eff}} = \sum_{n=1}^{\infty} \frac{k_n}{\mathcal{D}_0^2 \lambda_n^2 \delta^2 \left(\Delta - \frac{\delta}{3}\right)} \left[ e^{-\mathcal{D}_0 \lambda_n (\Delta + \delta)} + e^{-\mathcal{D}_0 \lambda_n (\Delta - \delta)} \right. \\ 519 \quad \left. - 2 \left( \mathcal{D}_0 \lambda_n \delta + e^{-\mathcal{D}_0 \lambda_n \delta} + e^{-\mathcal{D}_0 \lambda_n \Delta} - 1 \right) \right]$$

521 The single layer potential representation gives

$$522 \quad (103) \quad D_{ave}^{\text{eff}} = \mathcal{D}_0 - \frac{16}{35} \frac{\mathcal{D}_0^{3/2}}{\delta^2 (3\Delta - \delta) \sqrt{\pi}} \left[ (\Delta - \delta)^{7/2} + (\Delta + \delta)^{7/2} - 2 \left( \delta^{7/2} + \Delta^{7/2} \right) \right] \frac{|\Gamma|}{d|\Omega|} \\ 523 \quad + O(\Delta).$$

524 The mixed approximation in (89) gives

$$525 \quad (104) \quad D_{ave}^{\text{eff}} = \frac{\mathcal{D}_0 \delta}{6 \left(\Delta - \frac{\delta}{3}\right)} - \frac{8 \mathcal{D}_0^{3/2} \delta^{3/2}}{35 \sqrt{\pi} \left(\Delta - \frac{\delta}{3}\right) d|\Omega|} \\ - \sum_{n=1}^{\infty} \frac{\delta k_n + j_n}{\delta^2 \left(\Delta - \frac{\delta}{3}\right)} \left( \delta - \frac{e^{-\lambda_n \mathcal{D}_0 \Delta} (1 - e^{\lambda_n \mathcal{D}_0 \delta})}{\lambda_n \mathcal{D}_0} \right) \\ 526 \quad + O \left( \max \left\{ \frac{\delta^2}{\left(\Delta - \frac{\delta}{3}\right)}, \frac{\delta (\Delta - \delta)}{\left(\Delta - \frac{\delta}{3}\right)} \right\} \right).$$

527 **5. Numerical results.** In this Section we numerically validate the approximate  
 528 formulas we derived in the previous sections. To compute the reference quantities we  
 529 solved the diffusion equation in (17) using the Matlab PDEToolbox. The eigenvalues  
 530 and eigenfunctions of the Laplace equation with Neumann boundary conditions were  
 531 also computed with the same software. The convergence between the H-ADC model  
 532 and the Bloch-Torrey equation was shown previously in [14].

533 First we show the three approximations of  $h(t)$ . We consider a 2D geometry of one  
 534 vertically orientated ellipse with semi-axes of  $19\mu\text{m}$  and  $9\mu\text{m}$ . The intrinsic diffusion  
 535 coefficient is set to  $\mathcal{D}_0 = 1e^{-3}\text{mm}^2/\text{s}$  and we vary the values of  $\delta$ ,  $\Delta$  and  $\mathbf{u}_g$ . To  
 536 compute the reference solution  $h(t)$  we solved the problem (17) on the finite element  
 537 mesh shown in Fig. 2. The eigenvalues and eigenfunctions are also computed on the  
 538 same finite element mesh. The projections  $a_n$  and  $b_n$  are computed according to the  
 539 formulas in (25) and (81).

540 For this particular geometry the first four non-zero eigenvalues are

$$541 \quad \lambda_1 = 0.0097, \quad \lambda_2 = 0.0325, \quad \lambda_3 = 0.0383, \quad \lambda_4 = 0.0644,$$

542 and their numerically calculated projections  $a_i$  are reported in the table below.

543 Clearly, among the four eigenvalues, in the direction  $\mathbf{u}_g = [1, 0]$ , all but  $\lambda_3$  have  
 544 negligible contribution, and in the direction  $\mathbf{u}_g = [0, 1]$ , all but  $\lambda_1$  have negligible  
 545 contribution.

546 In the following plots we always indicate the reference quantity with a line, the  
 547 single layer approximation with squares, the eigenfunction approximation with circles  
 548 and the mixed approximation with asterisks.

549 In Figure 3 we considered  $\delta = 5\text{ms}$ ,  $\Delta = 10\text{ms}$  and  $\mathbf{u}_g = [1, 0]$ . As we can see  
 550 the single layer approximation (squares) fits very well the reference quantity (contin-  
 551 uous line) in all three time intervals. We also notice that the mixed approximation

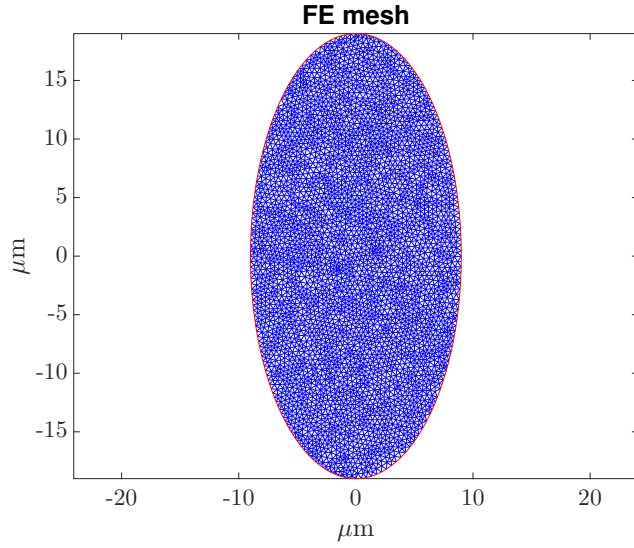


Fig. 2: Finite elements mesh of an ellipse with semiaxes of  $19\mu\text{m}$  and  $9\mu\text{m}$ , orientated vertically along the  $y$ -axis.

$\mathbf{u}_{\mathbf{g}}$	$a_1$	$a_2$	$a_3$	$a_4$
$[1, 0]$	38.9	-25.7	$-4.62e^{+5}$	-0.97
$[0, 1]$	$1.07e^{+6}$	1.75	-4.49	-5.58

Table 1: The first moments of the eigenfunction associated with the first four non-zero eigenvalues in the two directions  $\mathbf{u}_{\mathbf{g}} = [1, 0]$  and  $\mathbf{u}_{\mathbf{g}} = [0, 1]$ .

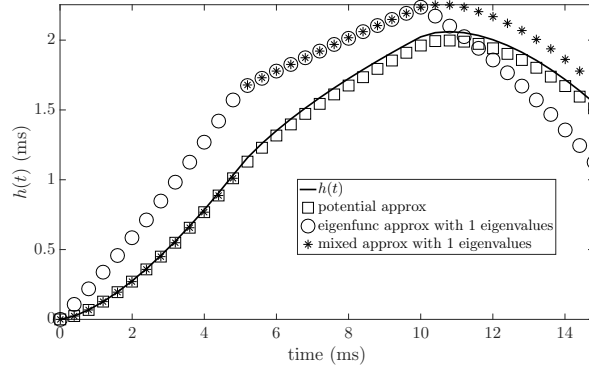


Fig. 3:  $h(t)$  and its approximation (using the three different formulas found) with respect to the gradient directions  $\mathbf{u}_{\mathbf{g}} = [1, 0]$  for an ellipse of semi-axes  $19\mu\text{m}$  and  $9\mu\text{m}$ . Intrinsic diffusion coefficients  $\mathcal{D}_0 = 1 \times 10^{-3}\text{mm}^2/\text{s}$ , pulses duration  $\delta = 5\text{ms}$  and time-delay between pulses  $\Delta = 10\text{ms}$ .

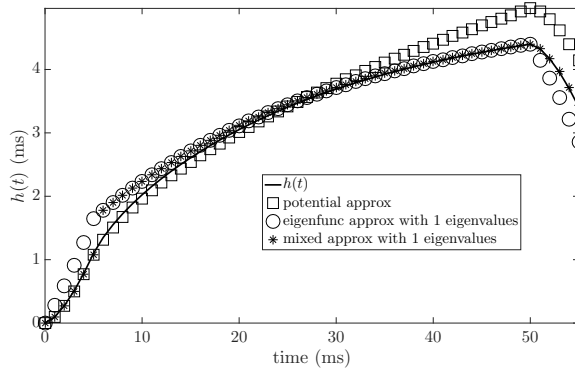


Fig. 4:  $h(t)$  and its approximation (using the three different formulas found) with respect to the gradient directions  $\mathbf{u}_g = [1, 0]$  for an ellipse of semiaxes  $19\mu\text{m}$  and  $9\mu\text{m}$ . Intrinsic diffusion coefficients  $\mathcal{D}_0 = 1 \times 10^{-3}\text{mm}^2/\text{s}$ , pulses duration  $\delta = 5\text{ms}$  and time-delay between pulses  $\Delta = 50\text{ms}$ .

552 (asterisks) works sufficiently well during the two pulses but not between them. For  
 553 the eigenfunctions approximation, the fit is far from the reference quantity.

554 In Figure 4 we considered  $\delta = 5\text{ms}$ ,  $\Delta = 50\text{ms}$  and  $\mathbf{u}_g = [1, 0]$ . As we can see the  
 555 single layer approximation fits well the reference quantity during the first pulse and  
 556 until  $t \approx 25\text{ms}$ , but after that, the approximation is no longer good. The eigenfunction  
 557 approximation is not good during the pulses but it becomes accurate at the end of  
 558 the interval between them. The mixed approximation fits well during the pulses and  
 559 is the same as the eigenfunction approximation between the pulses.

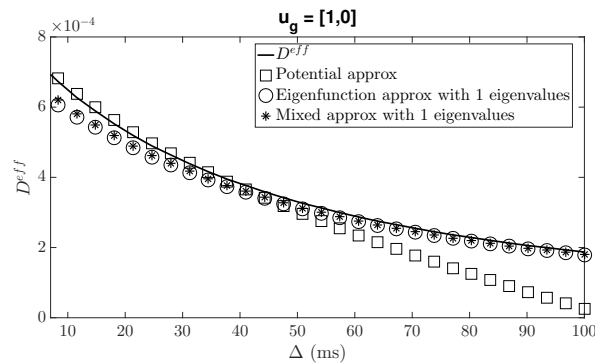
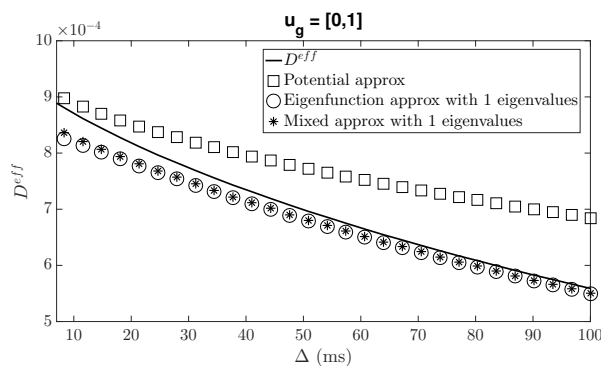
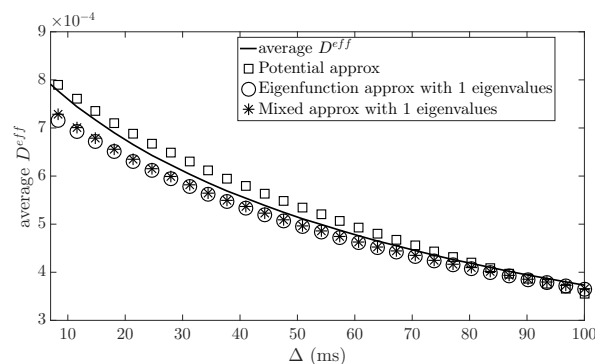
560 In Figures 5a and 5b we show the behaviour of  $D^{\text{eff}}$  computed for two different  
 561 directions of the gradient ( $\mathbf{u}_g = [1, 0]$  and  $\mathbf{u}_g = [0, 1]$ ) but the same parameters  
 562 ( $\delta = 5\text{ms}$  and thirty different values of  $\Delta$  equally distributed in the interval  $[8, 80]\text{ms}$ ).  
 563 In Figure 5c we show the average of  $D_{\text{ave}}^{\text{eff}}/\mathcal{D}_0$  along the two perpendicular directions.  
 564 Clearly, the single layer formula works well for at short  $\Delta + \delta$ , the eigenfunctions  
 565 formula for long  $\Delta + \delta$ .

566 To conclude, in Figure 6 we report the absolute error

$$567 \quad |D^{\text{eff}} - D^{\text{approx}}|$$

568 for the same parameters as before in the two orthogonal directions. As we can see,  
 569 the single layer approximation is better at short times and the eigenfunctions approx-  
 570 imation is better at long times. The time at which the switch between the short and  
 571 the long diffusion time approximations occurs at around  $t = 50\text{ms}$  in the direction  
 572  $[1, 0]$  and it occurs at around  $t = 25\text{ms}$  in the direction  $[0, 1]$ .

573 **6. Conclusions.** Diffusion Magnetic Resonance Imaging (dMRI) can be used to  
 574 measure a time and direction dependent effective diffusion coefficient which can in turn  
 575 reveal information about the tissue micro-structure. Recently a new mathematical  
 576 model for the effective diffusion coefficient, the H-ADC model, was obtained using  
 577 homogenization techniques after imposing a certain scaling relationship between the  
 578 physical parameters. The resulting model depends on the solution of a diffusion  
 579 equation subject to time-dependent Neumann boundary conditions.

(a) Gradient direction  $\mathbf{u}_g = [1, 0]$ (b) Gradient direction  $\mathbf{u}_g = [0, 1]$ 

(c) Average over both directions

Fig. 5:  $D^{\text{eff}}$  with respect to two different gradient directions as well as  $D_{\text{ave}}^{\text{eff}}$ , the average over both direction, compared to approximations using the three different formulas, for an ellipse of semiaxes  $19\mu\text{m}$  and  $9\mu\text{m}$ . Intrinsic diffusion coefficients  $D_0 = 1 \times 10^{-3}\text{mm}^2/\text{s}$ , pulses duration  $\delta = 5\text{ms}$  and thirty different values of the time-delay between pulses in the interval  $[8, 80]\text{ms}$ .

580 In this paper, we analysed the H-ADC model in the case of finite sub-domains.  
 581 In particular, we obtained three representations of the effective diffusion coefficient

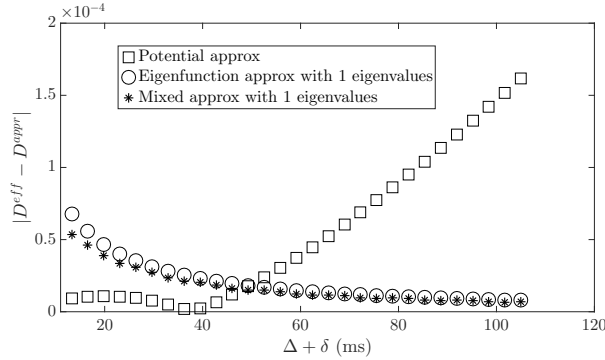
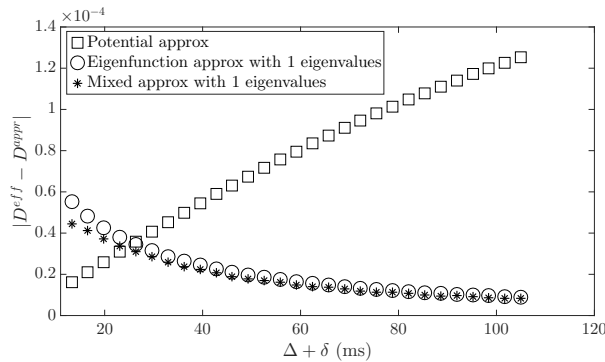

 (a) Gradient direction  $\mathbf{u}_g = [1, 0]$ 

 (b) Gradient direction  $\mathbf{u}_g = [0, 1]$ 

Fig. 6: Absolute error  $|D^{\text{eff}} - D^{\text{approx}}|$  using the three different formulas found with respect to two different gradient directions for an ellipse of semi-axes  $19\mu\text{m}$  and  $9\mu\text{m}$ . Intrinsic diffusion coefficients  $\mathcal{D}_0 = 1 \times 10^{-3}\text{mm}^2/\text{s}$ , pulses duration  $\delta = 5\text{ms}$  and thirty different values of the time-delay between pulses in the interval  $[8, 80]\text{ms}$ .

582 that are appropriate in different diffusion time regimes. In the short time regime, we  
 583 proposed using a representation based on the single layer potential. In the long time  
 584 regime when the pulse duration is not short, we proposed using a representation based  
 585 on the eigenfunctions expansion of the Neumann Laplace operator. In the long time  
 586 regime when the pulse duration is short, we proposed a representation that combines  
 587 the single layer potential during the pulses with the eigenfunction expansion between  
 588 the pulses. In particular, in the short time regime, our representation corrects an  
 589 existing formula by correctly accounting for the pulse duration. Our work helps to  
 590 make more precise how parameters of the tissue micro-structure such as the surface to  
 591 volume ratio or the dominant eigenvalue and its projection affect the effective diffusion  
 592 coefficient.

593

## REFERENCES

- 594 [1] S. AXELROD AND P. N. SEN, Nuclear magnetic resonance spin echoes for restricted diffusion  
 595 in an inhomogeneous field: Methods and asymptotic regimes, The Journal of Chemical  
 596 Physics, 114 (2001), p. 6878, <http://link.aip.org/link/?JCPA6/114/6878/1>.

- 597 [2] A. V. BARZYKIN, Theory of spin echo in restricted geometries under a step-wise gradient  
 598 pulse sequence, Journal of Magnetic Resonance, 139 (1999), pp. 342–353, [http://www.](http://www.sciencedirect.com/science/article/pii/S1090780799917780)  
 599 [sciencedirect.com/science/article/pii/S1090780799917780](http://www.sciencedirect.com/science/article/pii/S1090780799917780).
- 600 [3] L. M. BURCAW, E. FIEREMANS, AND D. S. NOVIKOV, Mesoscopic structure of neuronal  
 601 tracts from time-dependent diffusion, NeuroImage, 114 (2015), pp. 18 – 37, [https:](https://doi.org/http://dx.doi.org/10.1016/j.neuroimage.2015.03.061)  
 602 [//doi.org/http://dx.doi.org/10.1016/j.neuroimage.2015.03.061](https://doi.org/http://dx.doi.org/10.1016/j.neuroimage.2015.03.061), [http://www.sciencedirect.](http://www.sciencedirect.com/science/article/pii/S1053811915002578)  
 603 [com/science/article/pii/S1053811915002578](http://www.sciencedirect.com/science/article/pii/S1053811915002578).
- 604 [4] P. T. CALLAGHAN, A. COY, D. MACGOWAN, K. J. PACKER, AND F. O. ZELAYA, Diffraction-like  
 605 effects in nmr diffusion studies of fluids in porous solids, Nature, 351 (1991), pp. 467–469,  
 606 <http://dx.doi.org/10.1038/351467a0>.
- 607 [5] J. CHEN, W. LIU, H. ZHANG, L. LACY, X. YANG, S.-K. SONG, S. A. WICKLINE, AND  
 608 X. YU, Regional ventricular wall thickening reflects changes in cardiac fiber and sheet  
 609 structure during contraction: quantification with diffusion tensor MRI, American Journal  
 610 of Physiology - Heart and Circulatory Physiology, 289 (2005), pp. H1898–H1907,  
 611 <https://doi.org/10.1152/ajpheart.00041.2005>.
- 612 [6] J. CHEN, S.-K. SONG, W. LIU, M. MCLEAN, J. S. ALLEN, J. TAN, S. A. WICKLINE, AND X. YU,  
 613 Remodeling of cardiac fiber structure after infarction in rats quantified with diffusion tensor  
 614 MRI, American Journal of Physiology - Heart and Circulatory Physiology, 285 (2003),  
 615 pp. H946–H954, <https://doi.org/10.1152/ajpheart.00889.2002>.
- 616 [7] H. CHENG AND S. TORQUATO, Effective conductivity of periodic arrays of spheres with interfacial  
 617 resistance, Proceedings: Mathematical, Physical and Engineering Sciences, 453 (1997),  
 618 pp. 145–161, <http://www.jstor.org/stable/52987>.
- 619 [8] E. FIEREMANS, L. M. BURCAW, H.-H. LEE, G. LEMBERSKIY, J. VERAART, AND D. S. NOVIKOV,  
 620 In vivo observation and biophysical interpretation of time-dependent diffusion in human  
 621 white matter, NeuroImage, 129 (2016), pp. 414 – 427, [https://doi.org/http://dx.doi.](https://doi.org/http://dx.doi.org/10.1016/j.neuroimage.2016.01.018)  
 622 [org/10.1016/j.neuroimage.2016.01.018](https://doi.org/http://dx.doi.org/10.1016/j.neuroimage.2016.01.018), [http://www.sciencedirect.com/science/article/pii/](http://www.sciencedirect.com/science/article/pii/S1053811916000240)  
 623 [S1053811916000240](http://www.sciencedirect.com/science/article/pii/S1053811916000240).
- 624 [9] D. GREBENKOV, NMR survey of reflected brownian motion, Reviews of Modern Physics, 79  
 625 (2007), pp. 1077–1137, <http://dx.doi.org/10.1103/RevModPhys.79.1077>.
- 626 [10] D. GREBENKOV, Laplacian eigenfunctions in NMR. I. A numerical tool, Concepts in Magnetic  
 627 Resonance Part A, 32A (2008), pp. 277–301, <http://dx.doi.org/10.1002/cmr.a.20117>.
- 628 [11] D. S. GREBENKOV, Laplacian eigenfunctions in NMR. II. Theoretical advances, Concepts  
 629 Magn. Reson., 34A (2009), pp. 264–296, <http://dx.doi.org/10.1002/cmr.a.20145>.
- 630 [12] L. GREENGARD AND J. STRAIN, A fast algorithm for the evaluation of heat potentials, Comm.  
 631 Pure Appl. Math., 43 (1990), pp. 949–963.
- 632 [13] R. B. GUENTHER AND J. W. LEE, Partial differential equations of mathematical physics and  
 633 integral equations, Prentice Hall, Inglewood Cliffs, New Jersey, 1988.
- 634 [14] H. HADDAR, J.-R. LI, AND S. SCHIAVI, A Macroscopic Model for the Diffusion MRI Signal Accounting for Time-Dependent Diffusivity,  
 635 SIAM Journal on Applied Mathematics, 76 (2016), pp. 930–949, [https:](https://doi.org/10.1137/15M1019398)  
 636 [//doi.org/10.1137/15M1019398](https://doi.org/10.1137/15M1019398), <http://dx.doi.org/10.1137/15M1019398>, [https:](https://arxiv.org/abs/http://dx.doi.org/10.1137/15M1019398)  
 637 [//arxiv.org/abs/http://dx.doi.org/10.1137/15M1019398](https://arxiv.org/abs/http://dx.doi.org/10.1137/15M1019398).
- 638 [15] D. HASSELMAN AND L. F. JOHNSON, Effective thermal conductivity of composites with  
 639 interfacial thermal barrier resistance, Journal of Composite Materials, 21 (1987), pp. 508–  
 640 515.
- 641 [16] V. KENKRE, Simple solutions of the Torrey-Bloch equations in the NMR study of molecular  
 642 diffusion, Journal of Magnetic Resonance, 128 (1997), pp. 62–69, [http://dx.doi.org/10.](http://dx.doi.org/10.1006/jmre.1997.1216)  
 643 [1006/jmre.1997.1216](http://dx.doi.org/10.1006/jmre.1997.1216).
- 644 [17] V. G. KISELEV, The cumulant expansion: an overarching mathematical framework for  
 645 understanding diffusion nmr, Diffusion MRI: Theory, Methods, and Applications:  
 646 Theory, Methods, and Applications, (2010), p. 152, [http://books.google.com/books?hl=](http://books.google.com/books?hl=en&lr=&id=dbZCMePD52AC&oi=fnd&pg=PA152&dq=The+cumulant+expansion:+an+overarching+mathematical+framework+for+understanding+diffusion+NMR&ots=YI6BKXffDr&sig=WoLmTLw7ZGATkUe-g3EGbtz79I)  
 647 [en&lr=&id=dbZCMePD52AC&oi=fnd&pg=PA152&dq=The+c](http://books.google.com/books?hl=en&lr=&id=dbZCMePD52AC&oi=fnd&pg=PA152&dq=The+cumulant+expansion:+an+overarching+mathematical+framework+for+understanding+diffusion+NMR&ots=YI6BKXffDr&sig=WoLmTLw7ZGATkUe-g3EGbtz79I)  
 648 [umulant+expansion:+an+overarching+mathematical+framework+for+understanding+](http://books.google.com/books?hl=en&lr=&id=dbZCMePD52AC&oi=fnd&pg=PA152&dq=The+cumulant+expansion:+an+overarching+mathematical+framework+for+understanding+diffusion+NMR&ots=YI6BKXffDr&sig=WoLmTLw7ZGATkUe-g3EGbtz79I)  
 649 [diffusion+NMR&ots=YI6BKXffDr&sig=WoLmTLw7ZGATkUe-g3EGbtz79I](http://books.google.com/books?hl=en&lr=&id=dbZCMePD52AC&oi=fnd&pg=PA152&dq=The+cumulant+expansion:+an+overarching+mathematical+framework+for+understanding+diffusion+NMR&ots=YI6BKXffDr&sig=WoLmTLw7ZGATkUe-g3EGbtz79I).
- 650 [18] L. L. LATOUR, P. P. MITRA, R. L. KLEINBERG, AND C. H. SOTAK, Time-dependent diffusion  
 651 coefficient of fluids in porous media as a probe of surface-to-volume ratio, Journal of Mag-  
 652 netic Resonance, Series A, 101 (1993), pp. 342–346.
- 653 [19] L. L. LATOUR, K. SVOBODA, P. P. MITRA, AND C. H. SOTAK, Time-dependent diffusion of  
 654 water in a biological model system, Proceedings of the National Academy of Sciences, 91  
 655 (1994), pp. 1229–1233, <http://www.pnas.org/content/91/4/1229.abstract>.
- 656 [20] M. LAZAR, Mapping brain anatomical connectivity using white matter tractography, NMR  
 657 Biomed., 23 (2010), pp. 821–835, <http://dx.doi.org/10.1002/nbm.1579>.
- 658 [21] D. LE BIHAN AND H. JOHANSEN-BERG, Diffusion MRI at 25: Exploring brain tissue structure

- 659 and function, *NeuroImage*, 61 (2012), pp. 324–341, [http://www.sciencedirect.com/science/](http://www.sciencedirect.com/science/article/pii/S1053811911012857)  
 660 [article/pii/S1053811911012857](http://www.sciencedirect.com/science/article/pii/S1053811911012857).
- 661 [22] D. LEBIHAN, S.-I. URAYAMA, T. ASO, T. HANAKAWA, AND H. FUKUYAMA, Direct and fast  
 662 detection of neuronal activation in the human brain with diffusion mri, *PNAS*, 103 (2006),  
 663 pp. 8263–8268, <http://www.pnas.org/content/103/21/8263.abstract>.
- 664 [23] J.-R. LI, D. CALHOUN, C. POUPON, AND D. L. BIHAN, Numerical simulation of diffusion MRI signals using an adaptive time-stepping method,  
 665 Physics in Medicine and Biology, 59 (2014), p. 441, [http://stacks.iop.org/0031-9155/59/](http://stacks.iop.org/0031-9155/59/i=2/a=441)  
 666 [i=2/a=441](http://stacks.iop.org/0031-9155/59/i=2/a=441).
- 667 [24] J.-R. LI AND L. GREENGARD, High order accurate methods for the evaluation of layer heat  
 668 potentials, *SIAM J. Sci. Comput.*, 31 (2009), pp. 3847–3860, [https://doi.org/10.1137/](https://doi.org/10.1137/080732389)  
 669 [080732389](https://doi.org/10.1137/080732389), <http://dx.doi.org/10.1137/080732389>.
- 670 [25] S. E. MAIER, Y. SUN, AND R. V. MULKERN, Diffusion imaging of brain tumors, *NMR Biomed.*,  
 671 23 (2010), pp. 849–864, <http://dx.doi.org/10.1002/nbm.1544>.
- 672 [26] P. P. MITRA, P. N. SEN, AND L. M. SCHWARTZ, Short-time behavior of the diffusion coefficient  
 673 as a geometrical probe of porous media, *Phys. Rev. B*, 47 (1993), pp. 8565–8574, [https://](https://doi.org/10.1103/PhysRevB.47.8565)  
 674 [doi.org/10.1103/PhysRevB.47.8565](https://doi.org/10.1103/PhysRevB.47.8565), <http://link.aps.org/doi/10.1103/PhysRevB.47.8565>.
- 675 [27] P. P. MITRA, P. N. SEN, L. M. SCHWARTZ, AND P. LE DOUSSAL, Diffusion propagator as a  
 676 probe of the structure of porous media, *Physical review letters*, 68 (1992), pp. 3555–3558.
- 677 [28] M. E. MOSELEY, J. KUCHARCZYK, J. MINTOROVITCH, Y. COHEN, J. KURHANEWICZ, N. DERU-  
 678 GIN, H. ASGARI, AND D. NORMAN, Diffusion-weighted MR imaging of acute stroke:  
 679 correlation with T2- weighted and magnetic susceptibility-enhanced MR imaging in cats,  
 680 *AJNR Am J Neuroradiol*, 11 (1990), pp. 423–429, [http://www.ajnr.org/cgi/content/](http://www.ajnr.org/cgi/content/abstract/11/3/423)  
 681 [abstract/11/3/423](http://www.ajnr.org/cgi/content/abstract/11/3/423).
- 682 [29] C. H. NEUMAN, Spin echo of spins diffusing in a bounded medium, *The Journal of Chemical*  
 683 *Physics*, 60 (1974), p. 4508, <http://link.aip.org/link/?JCP/60/4508/1>.
- 684 [30] D. S. NOVIKOV, E. FIEREMANS, J. H. JENSEN, AND J. A. HELPERN, Random walks with barriers,  
 685 *Nat Phys*, 7 (2011), pp. 508–514, <http://dx.doi.org/10.1038/nphys1936>.
- 686 [31] D. S. NOVIKOV, J. H. JENSEN, J. A. HELPERN, AND E. FIEREMANS, Revealing  
 687 mesoscopic structural universality with diffusion, *Proceedings of the National Academy*  
 688 *of Sciences*, (2014), <https://doi.org/10.1073/pnas.1316944111>, [http://www.pnas.org/](http://www.pnas.org/content/early/2014/03/21/1316944111.abstract)  
 689 [content/early/2014/03/21/1316944111.abstract](http://www.pnas.org/content/early/2014/03/21/1316944111.abstract), [https://arxiv.org/abs/http://www.pnas.](https://arxiv.org/abs/http://www.pnas.org/content/early/2014/03/21/1316944111.full.pdf+html)  
 690 [org/content/early/2014/03/21/1316944111.full.pdf+html](https://arxiv.org/abs/http://www.pnas.org/content/early/2014/03/21/1316944111.full.pdf+html).
- 691 [32] D. S. NOVIKOV AND V. G. KISELEV, Effective medium theory of a diffusion-weighted signal,  
 692 *NMR in Biomedicine*, 23 (2010), pp. 682–697, <https://doi.org/10.1002/nbm.1584>, [http://](http://dx.doi.org/10.1002/nbm.1584)  
 693 [dx.doi.org/10.1002/nbm.1584](http://dx.doi.org/10.1002/nbm.1584).
- 694 [33] N. PYATIGORSKAYA, D. LEBIHAN, O. REYNAUD, AND L. CIOBANU, Relationship between the diffusion time and the diffusion MRI signal observed at 17.2 tesla in the healthy rat brain cortex,  
 695 *Magnetic Resonance in Medicine*, (2013), pp. n/a—n/a, [https://doi.org/10.1002/mrm.](https://doi.org/10.1002/mrm.24921)  
 696 [24921](https://doi.org/10.1002/mrm.24921), <http://dx.doi.org/10.1002/mrm.24921>.
- 697 [34] B. ROBERTSON, Spin-echo decay of spins diffusing in a bounded region, *Physical Review*, 151  
 698 (1966), p. 273, [http://prola.aps.org/abstract/PR/v151/i1/p273\\_1](http://prola.aps.org/abstract/PR/v151/i1/p273_1).
- 699 [35] D. ROHMER, A. SITEK, AND G. T. GULLBERG, Reconstruction and visualization of fiber and  
 700 sheet structure with regularized tensor diffusion MRI in the human heart, *Lawrence Berke-*  
 701 *ley National Laboratory Publication. LBNL-60277*, (2006).
- 702 [36] E. O. STEJSKAL AND J. E. TANNER, Spin diffusion measurements: Spin echoes in the presence of  
 703 a time-dependent field gradient, *The Journal of Chemical Physics*, 42 (1965), pp. 288–292,  
 704 <http://dx.doi.org/10.1063/1.1695690>.
- 705 [37] T. SUGAHARA, Y. KOROGI, M. KOCHI, I. IKUSHIMA, Y. SHIGEMATU, T. HIRAI, T. OKUDA,  
 706 L. LIANG, Y. GE, Y. KOMOHARA, Y. USHIO, AND M. TAKAHASHI, Usefulness of  
 707 diffusion-weighted MRI with echo-planar technique in the evaluation of cellularity in  
 708 gliomas, *J. Magn. Reson. Imaging*, 9 (1999), pp. 53–60, [http://dx.doi.org/10.1002/\(SICI\)](http://dx.doi.org/10.1002/(SICI)1522-2586(199901)9:1<53::AID-JMRI>3.0.CO;2-2)  
 709 [1522-2586\(199901\)9:1<53::AID-JMRI>3.0.CO;2-2](http://dx.doi.org/10.1002/(SICI)1522-2586(199901)9:1<53::AID-JMRI>3.0.CO;2-2).
- 710 [38] A. SZAFER, J. ZHONG, AND J. C. GORE, Theoretical model for water diffusion in tissues, *Magn.*  
 711 *Reson. Med.*, 33 (1995), pp. 697–712, <http://dx.doi.org/10.1002/mrm.1910330516>.
- 712 [39] S. TORQUATO AND M. D. RINTOUL, Effect of the interface on the properties of composite media,  
 713 *Phys. Rev. Lett.*, 75 (1995), pp. 4067–, [http://link.aps.org/doi/10.1103/PhysRevLett.75.](http://link.aps.org/doi/10.1103/PhysRevLett.75.4067)  
 714 [4067](http://link.aps.org/doi/10.1103/PhysRevLett.75.4067).
- 715 [40] Y. TSUSHIMA, A. TAKAHASHI-TAKETOMI, AND K. ENDO, Magnetic resonance (MR) differential  
 716 diagnosis of breast tumors using apparent diffusion coefficient (ADC) on 1.5-t, *J. Magn.*  
 717 *Reson. Imaging*, 30 (2009), pp. 249–255, <http://dx.doi.org/10.1002/jmri.21854>.
- 718 [41] D. S. TUCH, T. G. REESE, M. R. WIEGELL, AND V. J. WEDEEN, Diffusion MRI of complex  
 719 and function, *NeuroImage*, 61 (2012), pp. 324–341, [http://www.sciencedirect.com/science/](http://www.sciencedirect.com/science/article/pii/S1053811911012857)  
 720 [article/pii/S1053811911012857](http://www.sciencedirect.com/science/article/pii/S1053811911012857).

- 721        neural architecture, *Neuron*, 40 (2003), pp. 885–895.  
722 [42] S. WARACH, D. CHIEN, W. LI, M. RONTAL, AND R. R. EDELMAN, Fast magnetic resonance  
723 diffusion-weighted imaging of acute human stroke, *Neurology*, 42 (1992), pp. 1717–, [http:](http://www.neurology.org/cgi/content/abstract/42/9/1717)  
724 [//www.neurology.org/cgi/content/abstract/42/9/1717](http://www.neurology.org/cgi/content/abstract/42/9/1717).